NACA RM L55F30

NACA

RESEARCH MEMORANDUM

LONGITUDINAL AERODYNAMIC CHARACTERISTICS AT TRANSONIC SPEEDS OF A COMPLETE MODEL WITH AN UNSWEPT WING AND A SWEPTBACK HORIZONTAL TAIL AT TWO VERTICAL LOCATIONS

By Gerald Hieser and Louis Kudlacik

Langley Aeronautical Laboratory
Langley Field, Va.

NATIONAL ADVISORY COMMITTEE
FOR AERONAUTICS

WASHINGTON

September 1, 1955
Declassified November 20, 1959

NATIONAL ADVISORY COMMITTEE FOR AERONAUTICS

RESEARCH MEMORANDUM

LONGITUDINAL AERODYNAMIC CHARACTERISTICS AT TRANSONIC SPEEDS OF A COMPLETE MODEL WITH AN UNSWEPT WING AND A SWEPTBACK HORIZONTAL TAIL AT TWO VERTICAL LOCATIONS

By Gerald Hieser and Louis Kudlacik

SUMMARY

An investigation has been conducted to determine the static longitudinal stability contribution of a horizontal tail at two vertical locations behind a 4-percent-thick unswept-wing—fuselage combination at transonic speeds. Aerodynamic forces and moments were measured on the sting-supported model in the Langley 16-foot transonic tunnel at Mach numbers from 0.6 to 1.04 and at angles of attack from 0° to about 17°. The test Reynolds number based on the wing mean aerodynamic chord varied from about 4.6×10^6 to 6.0×10^6.

The model is comprised of an unswept wing located in the midwing position on a body of revolution and a sweptback horizontal tail mounted on a vertical tail.

The results of the investigation show that the stability contribution of the horizontal tail mounted at the 0.205 semispan position above the wing-chord plane was only about 40 percent of that for the tail mounted at the 0.614 semispan position above the wing-chord plane.

INTRODUCTION

A research program has been initiated at the Langley 16-foot transonic tunnel for the purpose of investigating the steady-state aerodynamic and loading characteristics, the longitudinal aerodynamic characteristics of the model with a horizontal tail, the fluctuating-flow properties, and the loading and effectiveness of lateral controls on a 4-percent-thick unswept-wing—fuselage combination at transonic speeds and high Reynolds numbers. The steady-state aerodynamic and loading characteristics are reported in reference 1.

The present report contains the longitudinal aerodynamic characteristics of the model with a sweptback horizontal tail. The experimental effective downwash is presented for two vertical locations of the tail behind the wing.

The sting-supported model used for this investigation has a wing with zero sweep of the 0.50-chord line, an aspect ratio of 4, a taper ratio of 0.5, and NACA 65A004 airfoil sections. The 45° sweptback horizontal tail has NACA 65A006 airfoil sections parallel to the plane of symmetry, an aspect ratio of 4, and a taper ratio of 0.6. The distance between the 0.25 mean-aerodynamic-chord points of the wing and tail was 121 percent of the wing semispan. The two vertical locations of the horizontal tail were 0.205 and 0.614 wing semispan above the wing-chord plane.

The model was tested at Mach numbers from 0.6 to 1.04 and angles of attack from 0° to about 17°. The Reynolds number, based on the wing mean aerodynamic chord, varied from 4.6×10^6 to 6.0×10^6.

SYMBOLS

C_L lift coefficient, $\frac{\text{Lift}}{qS}$

C_D drag coefficient, $\frac{\text{Drag}}{qS}$

C_m pitching-moment coefficient,

$$\frac{\text{Pitching moment about mean aerodynamic quarter chord}}{qS\bar{c}}$$

C_{m_t} tail contribution to pitching moment, $C_{m(\text{tail on})} - C_{m(\text{tail off})}$

C_{N_t} horizontal-tail normal-force coefficient, $\frac{\text{Normal force}}{qS_t}$

$C_{m_{i_t}} = \frac{\partial C_m}{\partial i_t}$

$C_{m_{i_{t_o}}} = \frac{\partial C_m}{\partial i_t}$ for wing-off tests at $\alpha = 0$

q free-stream dynamic pressure

q_t effective dynamic pressure at tail plane

S wing area

S_t horizontal-tail area

M free-stream Mach number

$\bar{c}$ mean aerodynamic chord, $\frac{2}{S}\int_0^{b/2} c^2 dy$

$\bar{c}_t$ mean aerodynamic chord of horizontal tail, $\frac{2}{S_t}\int_0^{b_t/2} c_t{}^2 dy$

c wing chord at any spanwise station

c_t horizontal-tail chord at any spanwise station

y lateral distance measured perpendicular to plane of symmetry

α angle of attack of model (referred to fuselage center line)

α_t effective angle of attack of horizontal tail

b wing span

b_t span of horizontal tail

h_t height of horizontal tail above wing-chord plane

P_b base-pressure coefficient, $\frac{p_b - p_o}{q}$

p_b static pressure at model base

p_o free-stream static pressure

i_t horizontal-tail incidence (angle with respect to fuselage center line)

l_t horizontal-tail length, distance from wing $\bar{c}/4$ to center of pressure of horizontal tail, measured parallel to fuselage center line

Λ sweepback angle

ϵ_e effective downwash angle at horizontal tail

$\Delta\epsilon_e$ increment in effective downwash angle from zero lift

MODEL AND APPARATUS

Model and instrumentation.- Geometric details and pertinent dimensions of the model are given in figure 1 and a photograph of the model mounted in the tunnel is shown as figure 2. The fuselage is a cylindrical body of revolution with an ogival nose and a slightly boattailed afterbody. A table of the fuselage ordinates is included in reference 1. The steel wing was mounted in a midwing position on the fuselage and has no geometric incidence, twist, or dihedral. The 45° sweptback horizontal tail was also fabricated of steel and has no geometric twist or dihedral. The vertical tail is not representative of an airplane configuration but was designed to permit support for the horizontal tail at various positions above the wing-chord plane.

The model forces and moments were measured by a six-component internal strain-gage balance. The model angle of attack was obtained from the static angle corrected for deflections due to load.

The model base pressures were measured by two orifices mounted flush with the internal surface of the fuselage and about 2 inches from the fuselage base.

Tunnel and model support.- The tests were conducted in the Langley 16-foot transonic tunnel which has an octagonal slotted test section that permits a continuous variation in speed to Mach numbers slightly above 1.0.

The sting-support system, which is described in reference 2, is arranged so that the model is located near the tunnel center line at all angles of attack.

TESTS

Measurements of the model forces and moments were obtained for the Mach numbers and angles of attack given in the following table:

Mach number, M	Angle of attack, α, deg at -		
	$\frac{h_t}{b/2} = 0.205$		$\frac{h_t}{b/2} = 0.614$
	$i_t = 0$	$i_t = -2^{\circ}$	$i_t = -2^{\circ}$
0.60	0 to 14.4	0 to 14.7	0 to 14.7
0.85	0 to 16.3	0 to 16.3	0 to 16.2
.90	0 to 16.5	0 to 14.4	0 to 16.4
.92	0 to 16.6	0 to 14.7	0 to 16.5
.94	0 to 17.0	0 to 14.9	0 to 16.9
.98	0 to 12.7	0 to 12.8	0 to 12.7
1.00	0 to 10.5	0 to 10.5	0 to 10.5
1.04	0 to 8.1	0 to 9.5	0 to 8.2

The tail normal force was measured through a tail-incidence range during tests with the wing off. These tests were conducted with the model at an angle of attack of 0° and with the horizontal tail mounted in the 0.614 semispan position.

The test Reynolds number based on wing mean aerodynamic chord varied from 4.6×10^6 to 6.0×10^6 over the test Mach number range.

ACCURACY

The measurement of Mach number in the test region is believed to be accurate within ± 0.005 (ref. 3), and the angles of attack presented are believed to be correct within $\pm 0.1^{\circ}$.

The lift and drag data have been adjusted to the condition of free-stream static pressure at the model base (base diameter = 6.28 inches). The variation of model base-pressure coefficient with angle of attack and Mach number is presented in figure 3 for the model with the horizontal tail at the 0.205 semispan position and an incidence of 0°. Changing the incidence or tail position had only a small effect on the base pressure.

No adjustments for sting interference or aeroelasticity have been applied to the aerodynamic forces and moments. The maximum twist of the wing for the range of test conditions reported have been estimated to be about 0.6°. (See ref. 1.) It is believed that the boundary-interference effects for wing-body combinations are generally negligible in this slotted test section at Mach numbers up to slightly above 1.0. (See

ref. 4.) The data presented at $M = 1.04$ may be affected somewhat by boundary-reflected disturbances impinging on the model; however, no attempt has been made to evaluate these effects. The accuracy of the measured coefficients based on balance accuracy and repeatability of data is believed to be within the following limits:

C_L	±0.01
C_D at low lift coefficients	±0.001
C_D at high lift coefficients	±0.003
C_m	±0.003

RESULTS AND DISCUSSION

Lift and drag data for the model with the horizontal tail at $\frac{h_t}{b/2} = 0.205$, $i_t = -2^\circ$ and 0°, and at $\frac{h_t}{b/2} = 0.614$, $i_t = -2^\circ$ are given in figures 4 and 5.

The pitching-moment data for the model configurations given above and for the model without the horizontal and vertical tails (obtained from the data of ref. 1) are presented in figure 6. These data indicate an increase in static longitudinal stability with increasing Mach number. This increase in stability results primarily from a rearward movement of the center of pressure on the wing as the Mach number is increased through the transonic range. (See ref. 1.)

A comparison of the data in figures 6(b) and 6(c) with the data of figure 6(d) shows that the angle of attack at which a reduction in the model stability occurs is greater with the tail at the 0.614 semispan position at Mach numbers up to 0.94. No reduction in stability is indicated for either tail position at Mach numbers above 0.94 and angles of attack up to the limit of the tests. The model is more stable at all Mach numbers with the tail located in the higher position throughout the angle-of-attack range investigated. This increased stability results from the fact that the higher tail is located farther from the wing wake center at these angles of attack and, therefore, operates in a lesser downwash field.

The tail effectiveness parameter $C_{m_{i_t}}$ is presented for the model with the tail at the 0.205 semispan position in figure 7. The effectiveness generally increases with Mach number until a Mach number of about 0.98 is reached, after which a slight decrease in effectiveness is indicated. Apparently this characteristic is predominantly the effect of Mach number on the tail lift-curve slope.

In order to obtain the relative magnitude of the downwash at the two tail positions, the effective downwash has been calculated from the equation $\epsilon_e = \alpha - \alpha_t + i_t$. For the lower tail position, α_t was obtained from the expression $C_{m_t}/C_{m_{i_t}}$. Because the model was tested with the tail at only one incidence angle for the 0.614 semispan tail position, α_t was obtained from the tail normal-force characteristics presented in figure 8. The expression $\dfrac{-C_{m_t}}{\frac{q_t}{q}\frac{S_t}{S}\frac{l_t}{\bar{c}}}$ was utilized to determine the horizontal-tail normal-force coefficient C_{N_t} at each test condition. The tail length l_t was determined from chordwise center-of-pressure data given in reference 5 for a wing of the same geometry as the present horizontal tail. The dynamic-pressure ratio q_t/q was extracted from reference 6.

In figure 9 the incremental effective downwash angle (downwash calculated at any angle of attack minus downwash calculated at $\alpha = 0^\circ$) is presented as a function of angle of attack and Mach number. Incremental values are presented because of the relatively high contribution of the tail empennage drag to C_{m_t}. The limited dynamic-pressure-ratio data of reference 6 prevented calculation of downwash for the 0.614 semispan tail position at angles of attack beyond 10°. The downwash parameter $\partial\Delta\epsilon_e/\partial\alpha$ measured between $\alpha = 0^\circ$ and $\alpha = 4^\circ$ is shown as a function of Mach number in figure 10. This parameter for the tail at $h_t/b_2 = 0.614$ is only about 60 percent of the value for the tail location at $h_t/b_2 = 0.205$, and the horizontal-tail contribution to stability for the low position is only about 40 percent of that for the tail in the high position.

CONCLUSION

Results of an investigation to determine the static longitudinal stability contribution of a horizontal tail located at two vertical positions behind a 4-percent-thick unswept-wing—fuselage combination at transonic speeds lead to the following conclusion:

The downwash parameter $\partial\Delta\epsilon_e/\partial\alpha$ for the tail located at 0.614 wing semispan above the wing-chord plane extended is only about 60 percent of the value for the tail located 0.205 semispan above the wing-chord plane. The horizontal-tail contribution to stability for the tail in the low position is only about 40 percent of that for the tail in the high position.

Langley Aeronautical Laboratory,
National Advisory Committee for Aeronautics,
Langley Field, Va., June 29, 1955.

REFERENCES

1. Hieser, Gerald, Henderson, James H., and Swihart, John M.: Transonic Aerodynamic and Loads Characteristics of a 4-Percent-Thick Unswept-Wing—Fuselage Combination. NACA RM L54B24, 1954.

2. Hallissy, Joseph M., and Bowman, Donald R.: Transonic Characteristics of a 45° Sweptback Wing-Fuselage Combination. Effect of Longitudinal Wing Position and Division of Wing and Fuselage Forces and Moments. NACA RM L52K04, 1953.

3. Ward, Vernon G., Whitcomb, Charles F., and Pearson, Merwin D.: Air-Flow and Power Characteristics of the Langley 16-Foot Transonic Tunnel With Slotted Test Section. NACA RM L52E01, 1952.

4. Whitcomb, Charles F., and Osborne, Robert S.: An Experimental Investigation of Boundary Interference on Force and Moment Characteristics of Lifting Models in the Langley 16- and 8-Foot Transonic Tunnels. NACA RM L52L29, 1953.

5. Hallissy, Joseph M., Jr., West, F. E., Jr., and Liner, George: Effects of Spoiler Ailerons on the Aerodynamic Load Distribution Over a 45° Sweptback Wing at Mach Numbers From 0.60 to 1.03. NACA RM L54C17a, 1954.

6. Myers, Boyd C., II, and Wiggins, James W.: Aerodynamic Characteristics of a Wing With Unswept Quarter-Chord Line, Aspect Ratio 4, Taper Ratio 0.6, and NACA 65A004 Airfoil Section. Transonic-Bump Method. NACA RM L50C16, 1950.

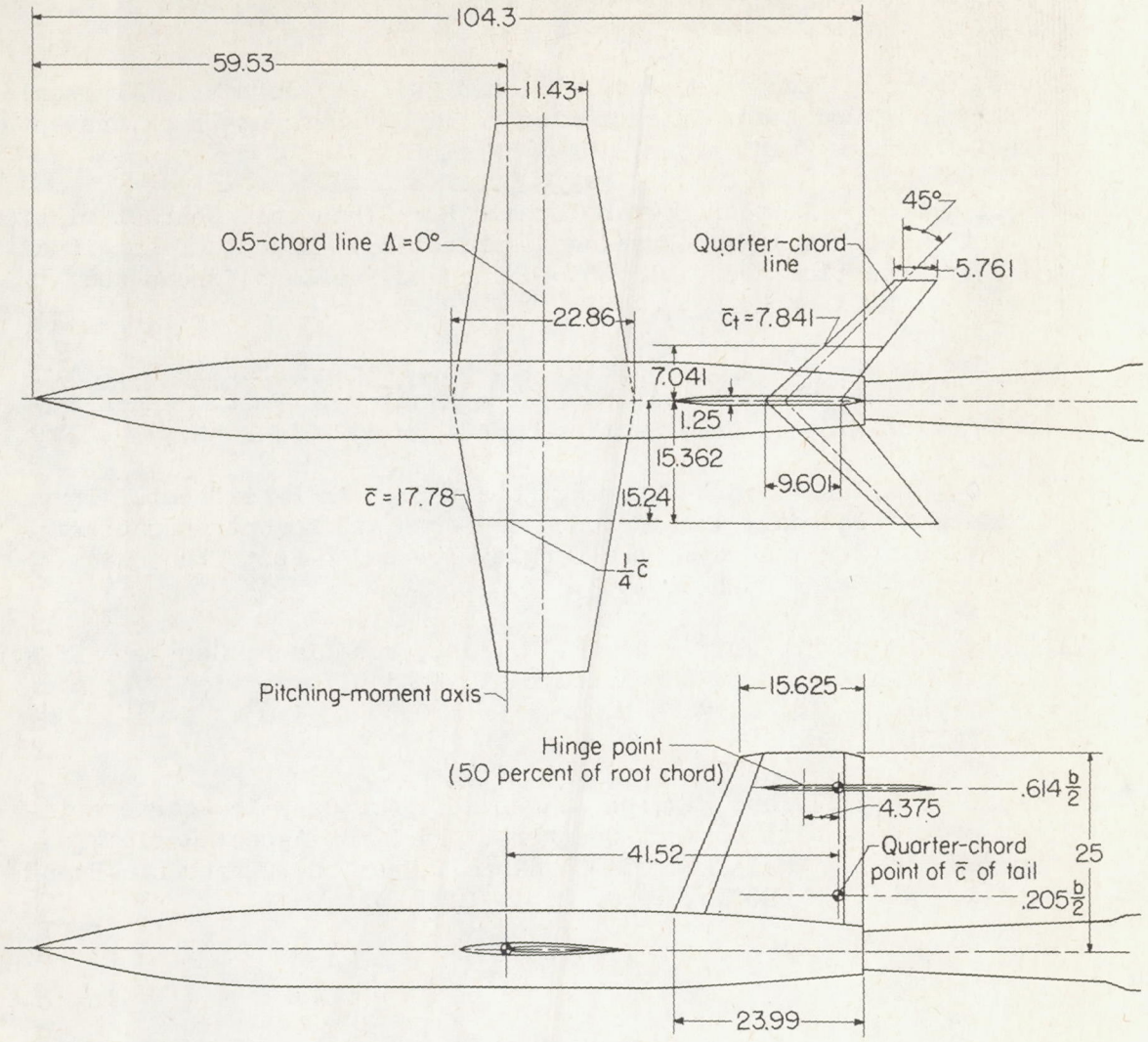

	Wing	Horizontal tail
Taper ratio	0.5	0.6
Aspect ratio	4.0	4.0
Area	8.165 sq ft	1.639 sq ft
Span	68.37 in.	30.724 in.
Airfoil	NACA 65A004 parallel to plane of symmetry	NACA 65A006 parallel to plane of symmetry
$\Lambda_{c/4}$	4.78°	45°

Figure 1.- Geometric details of model. All dimensions are in inches.

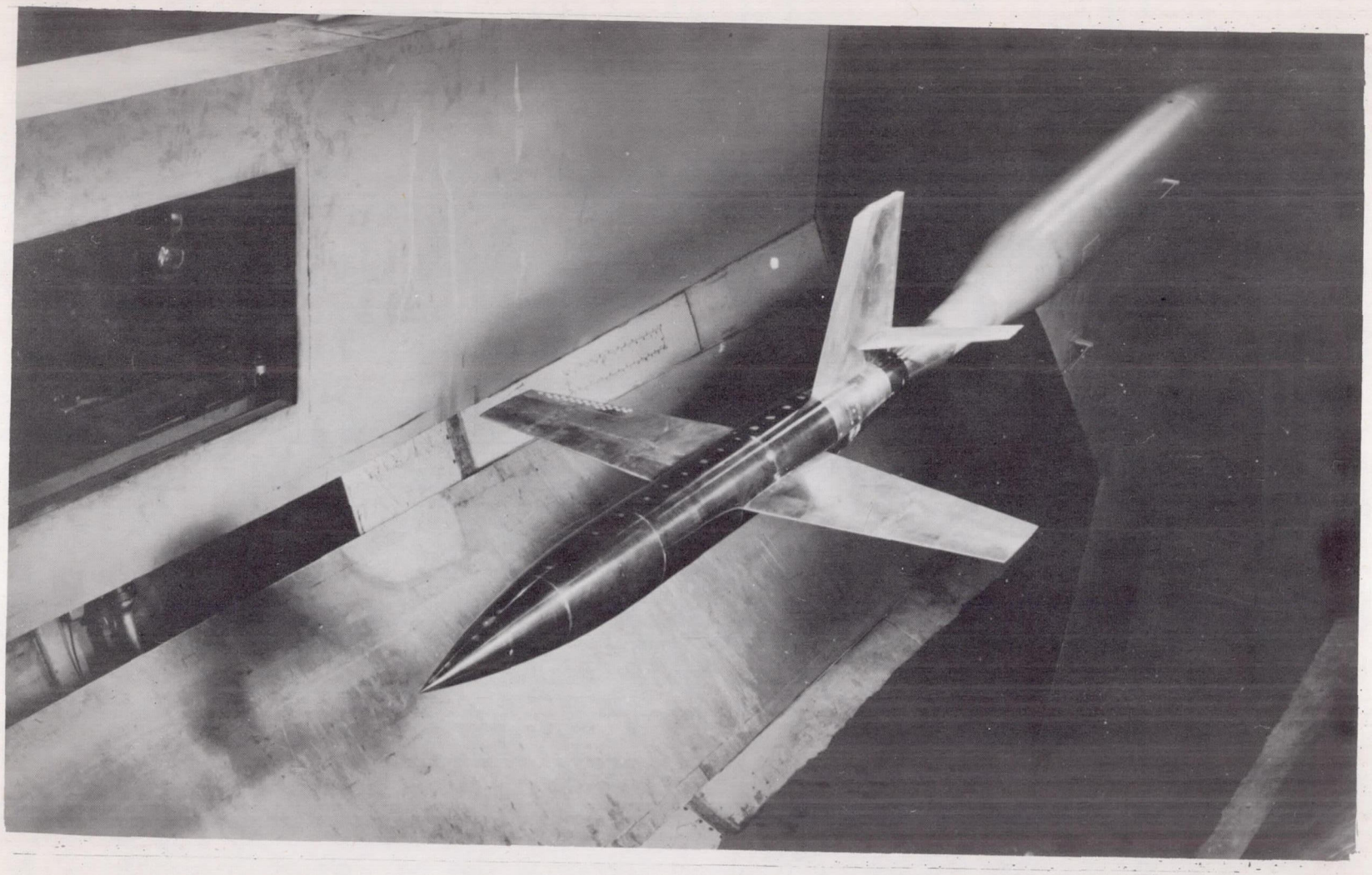

L-79961

Figure 2.- Photograph of model in the Langley 16-foot transonic tunnel.

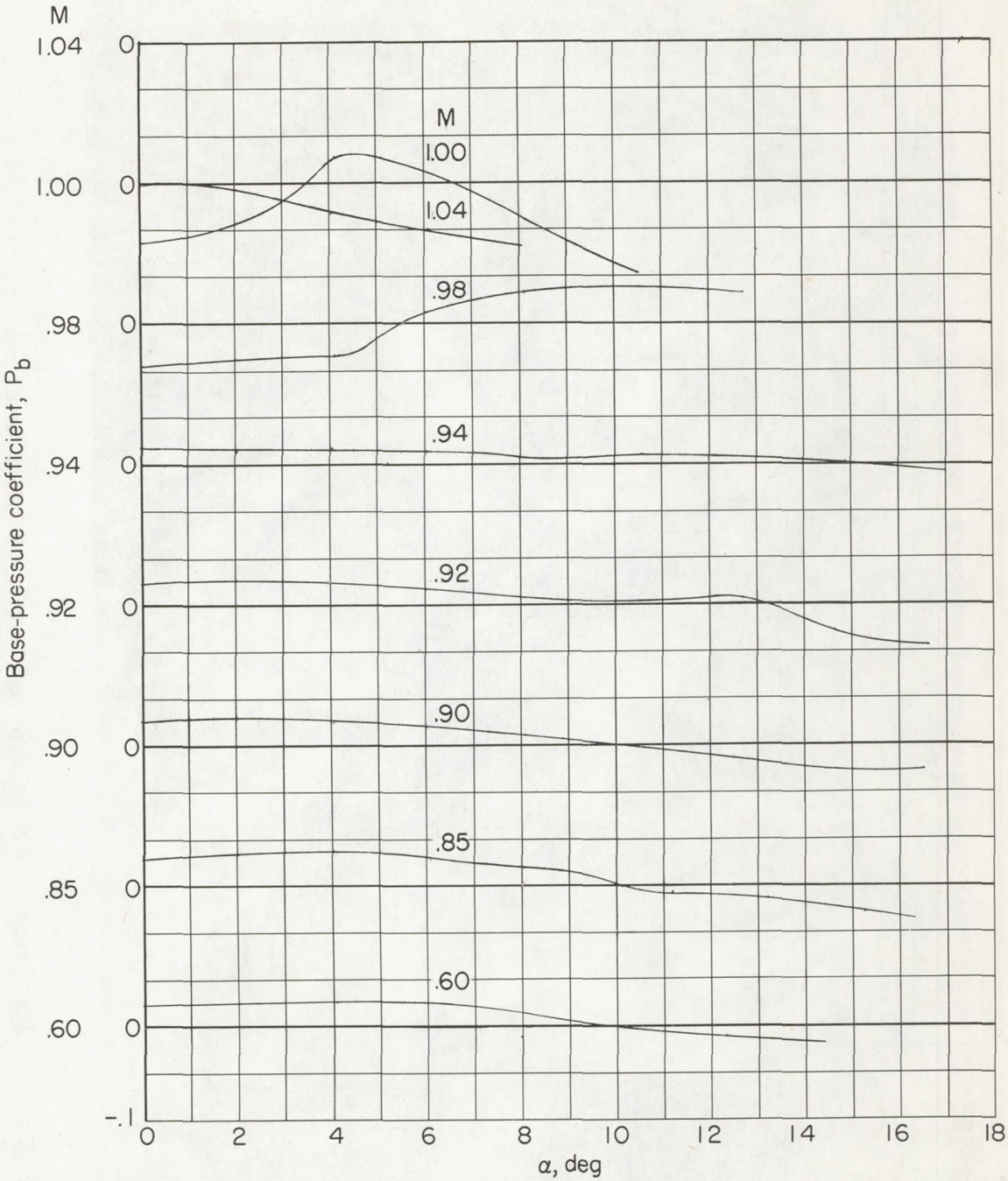

Figure 3.- Base-pressure coefficient. $\frac{h_t}{b/2} = 0.205$; $i_t = 0^{\circ}$.

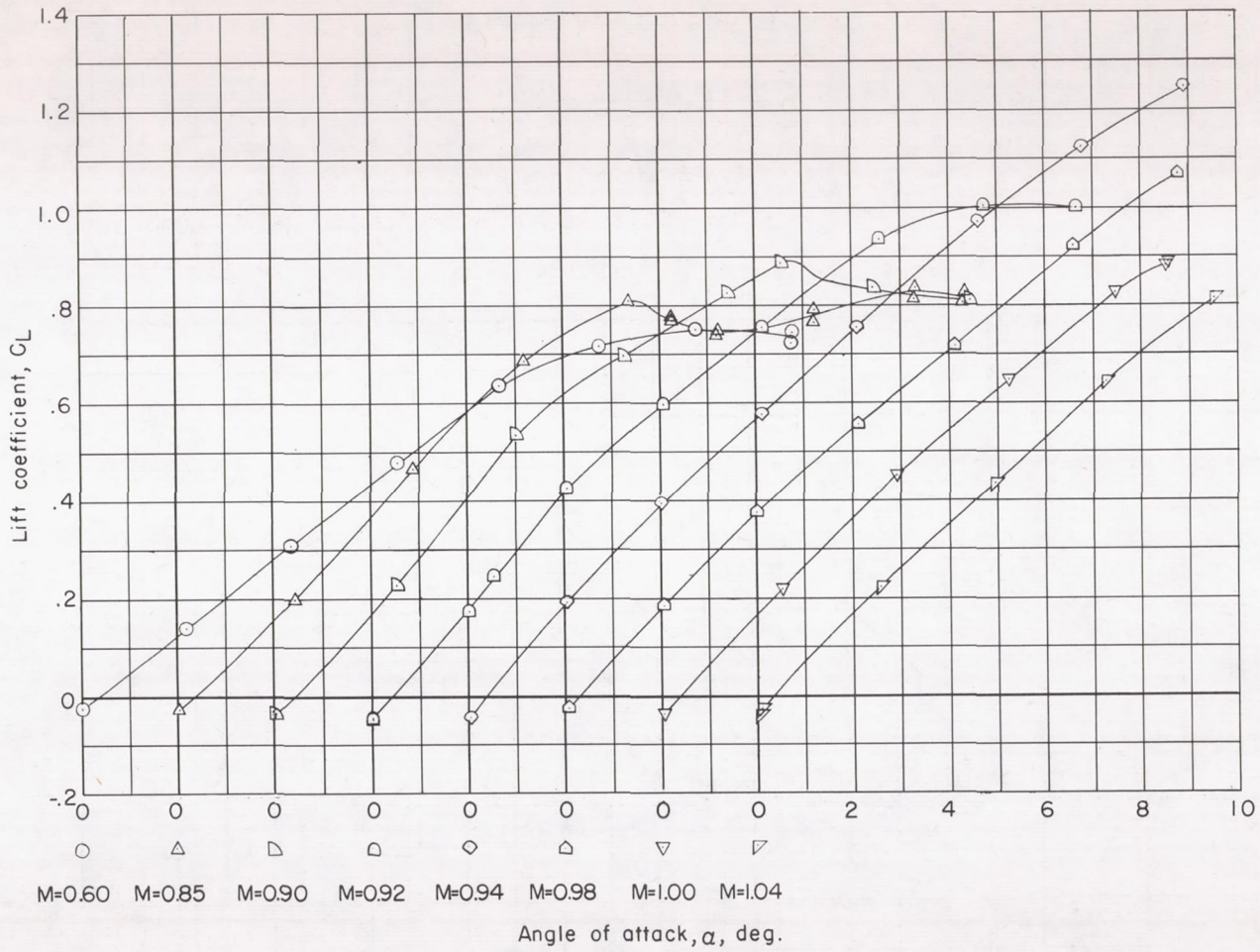

(a) $\frac{h_t}{b/2} = 0.205$; $i_t = -2^{\circ}$.

Figure 4.- Variation of lift coefficient with angle of attack.

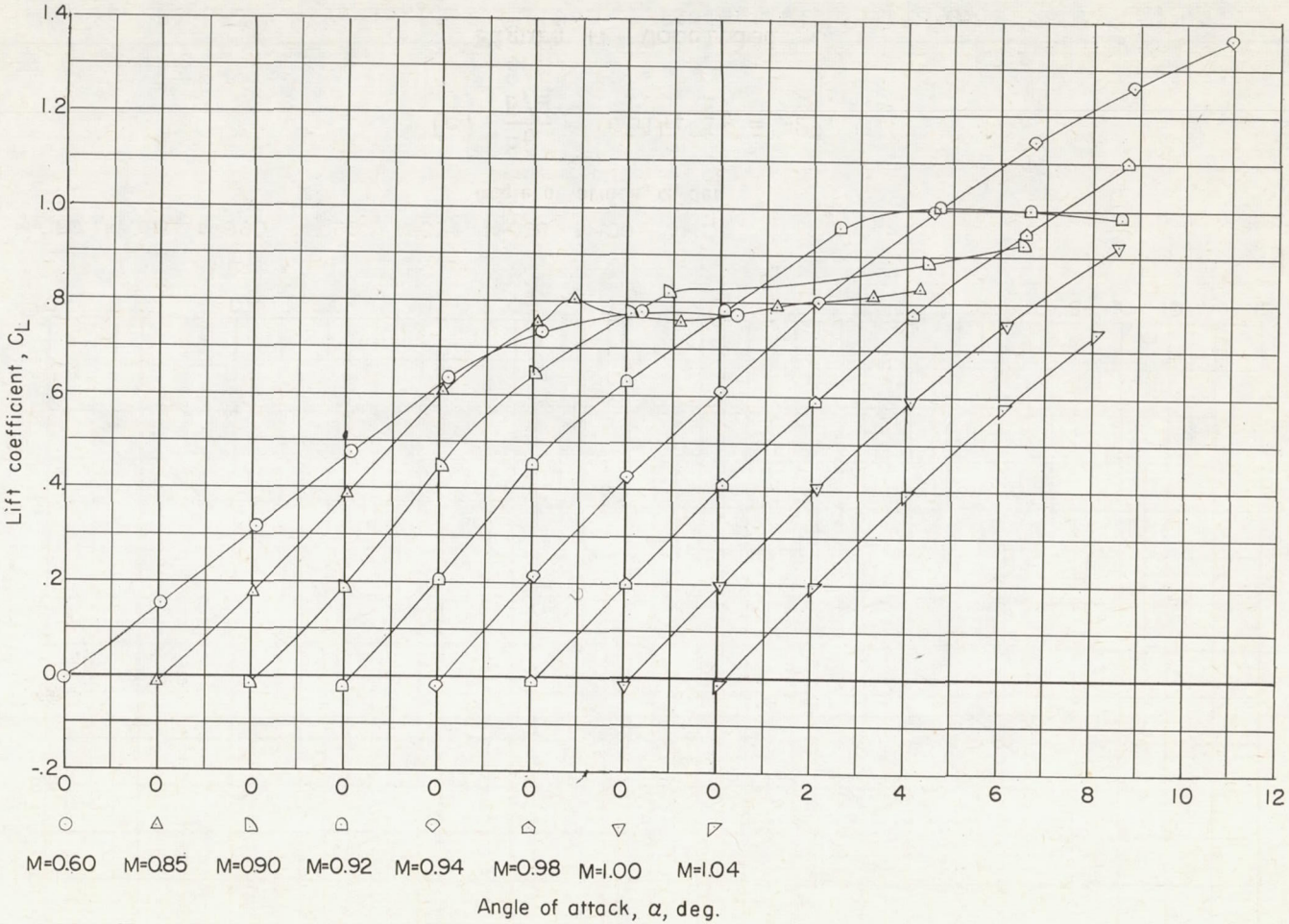

(b) $\frac{h_t}{b/2} = 0.205$; $i_t = 0^{\circ}$.

Figure 4.- Continued.

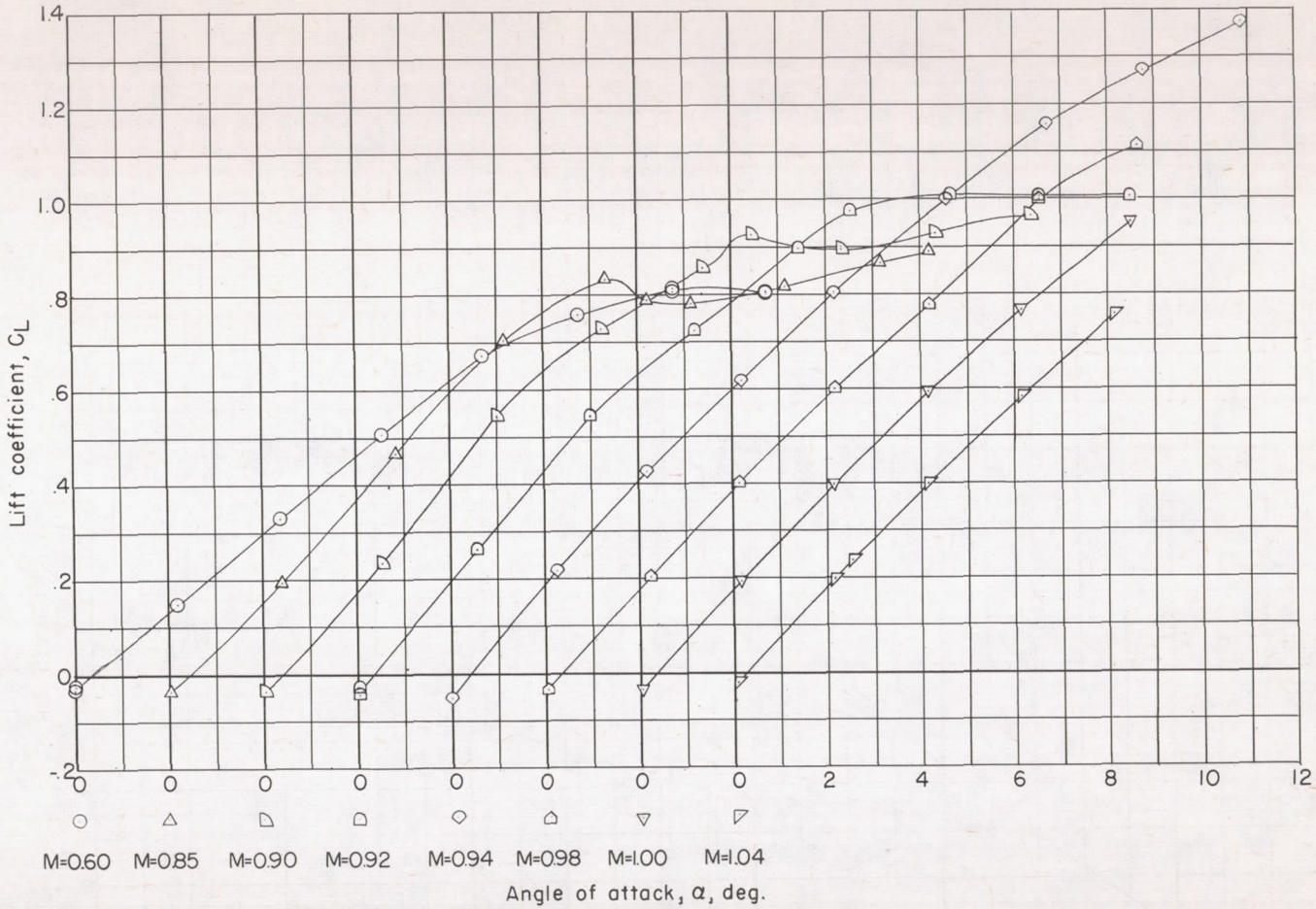

(c) $\frac{h_t}{b/2} = 0.614$; $i_t = -2^{\circ}$.

Figure 4.- Concluded.

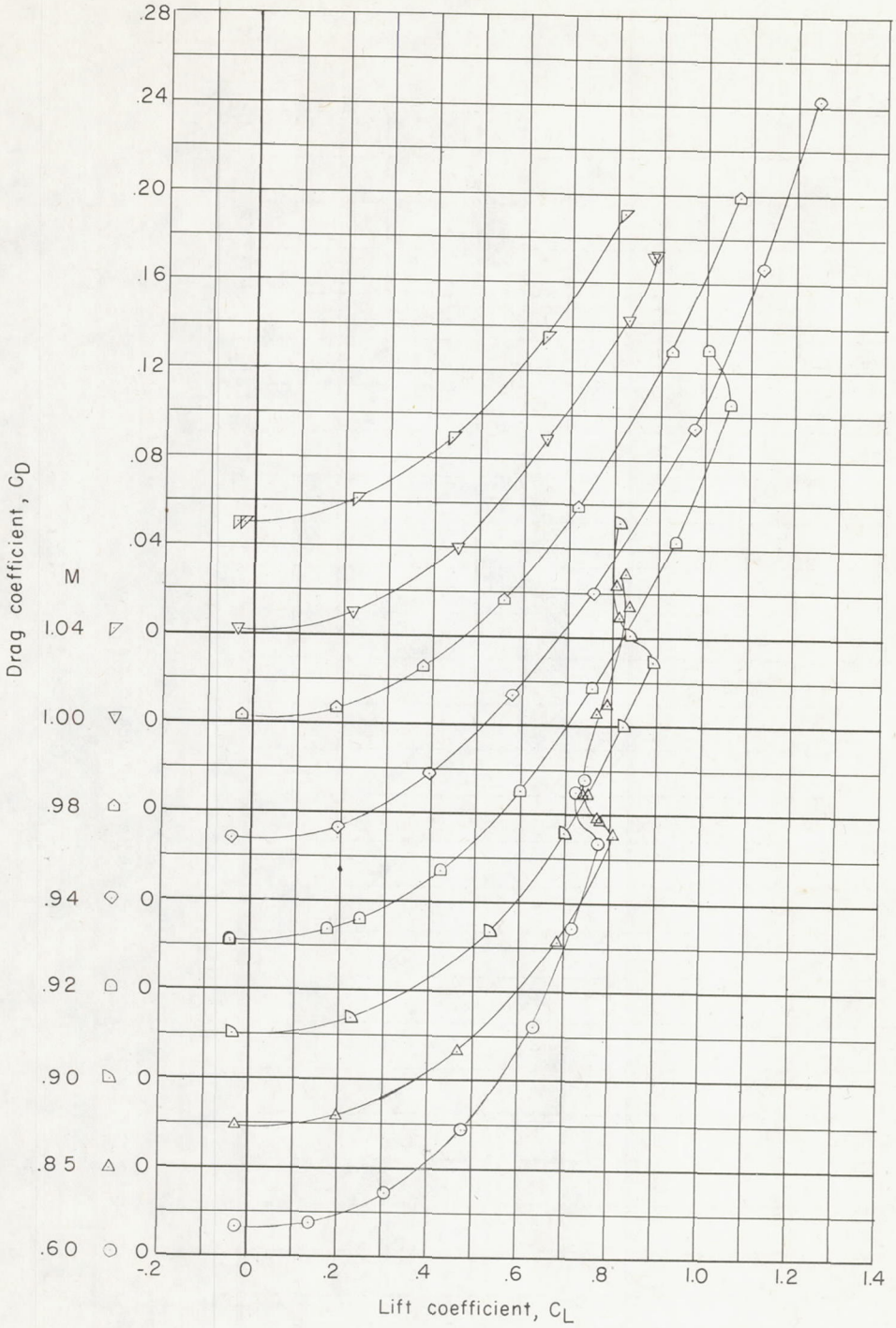

(a) $\frac{h_t}{b/2} = 0.205$; $i_t = -2^{\circ}$.

Figure 5.- Variation of drag coefficient with lift coefficient.

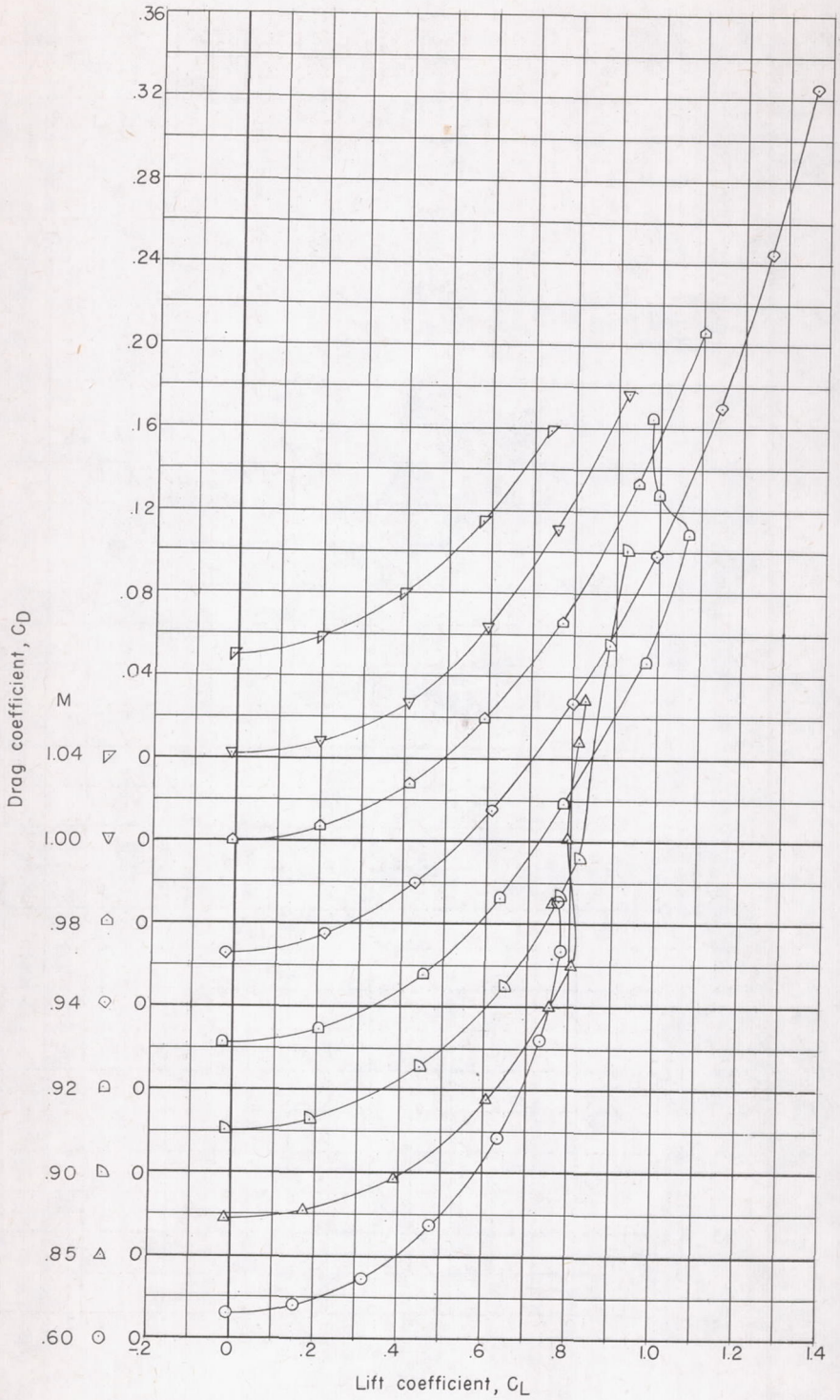

(b) $\frac{h_t}{b/2} = 0.205$; $i_t = 0^{\circ}$.

Figure 5.- Continued.

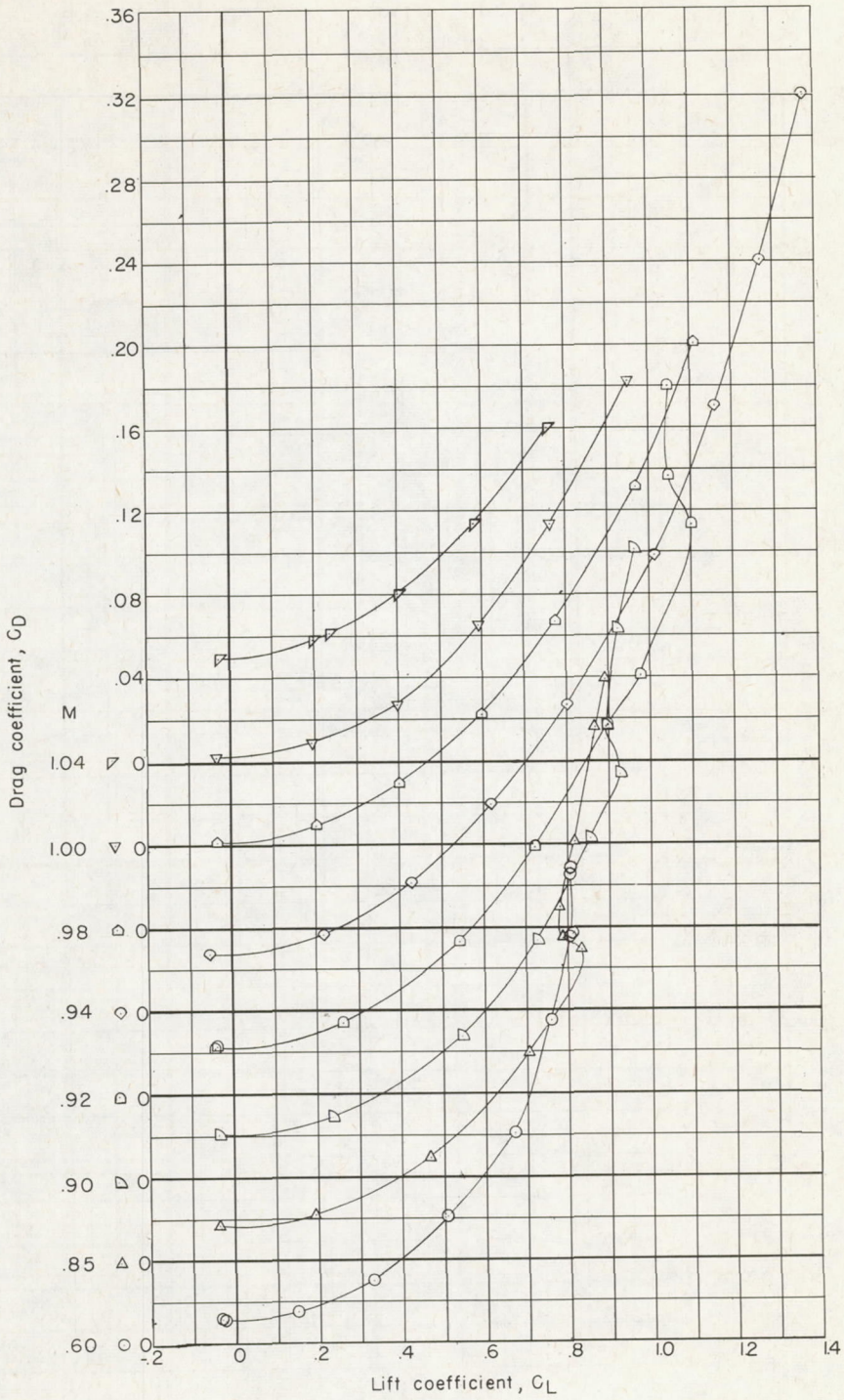

(c) $\frac{h_t}{b/2} = 0.614$; $i_t = -2^{\circ}$.

Figure 5.- Concluded.

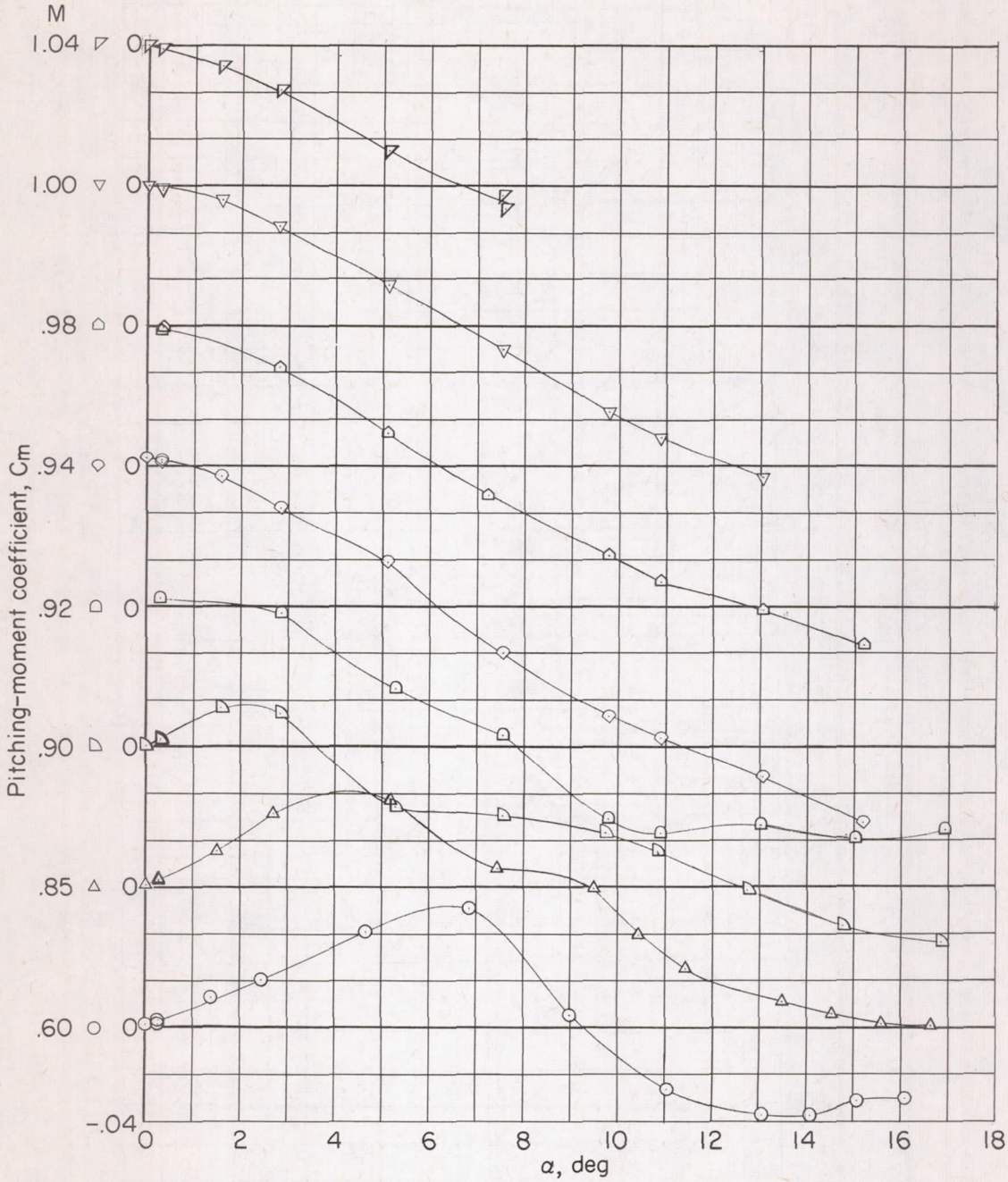

(a) Tail off.

Figure 6.- Variation of pitching-moment coefficient with angle of attack.

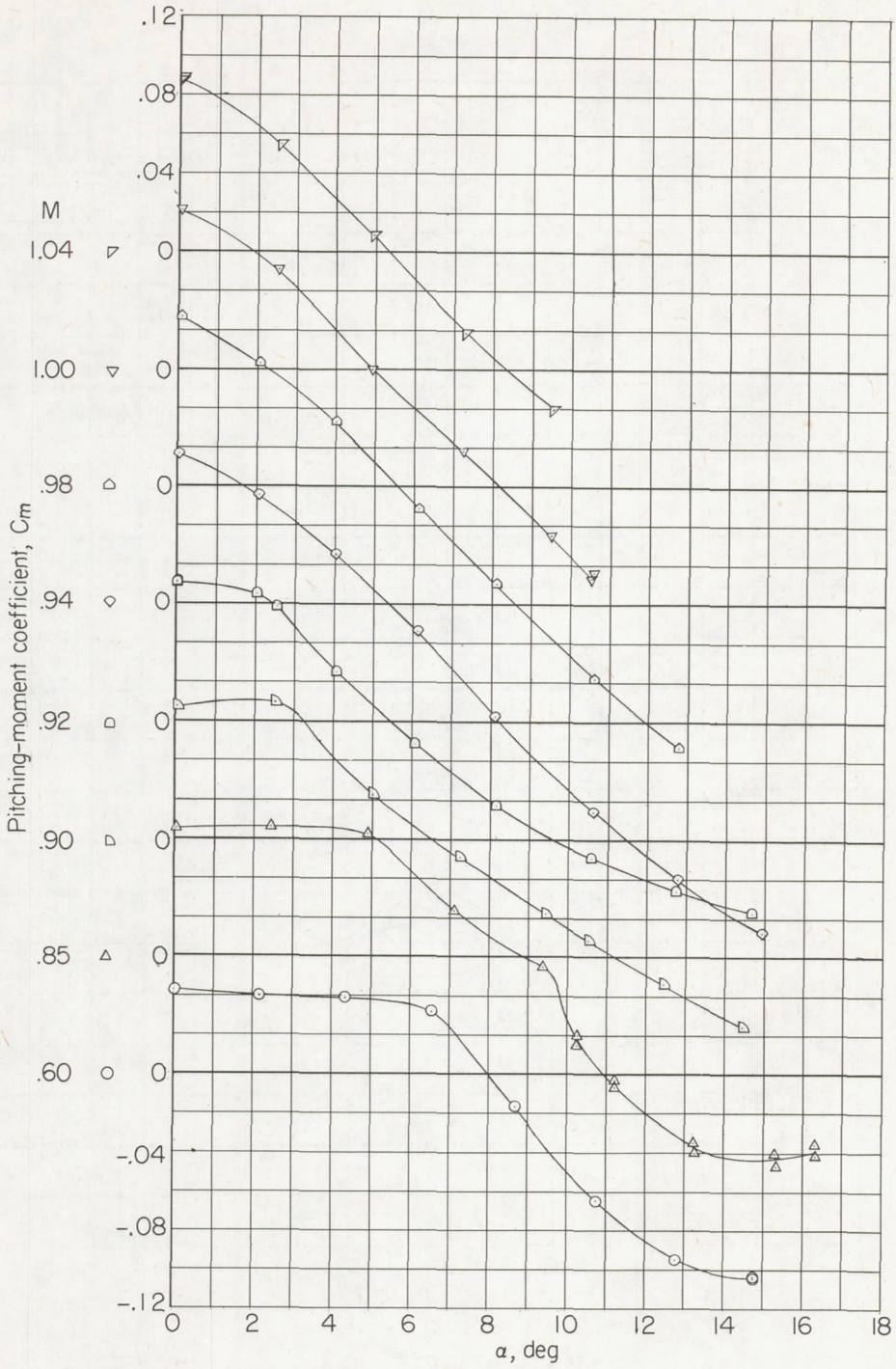

(b) $\frac{h_t}{b/2} = 0.205$; $i_t = -2^{\circ}$.

Figure 6.- Continued.

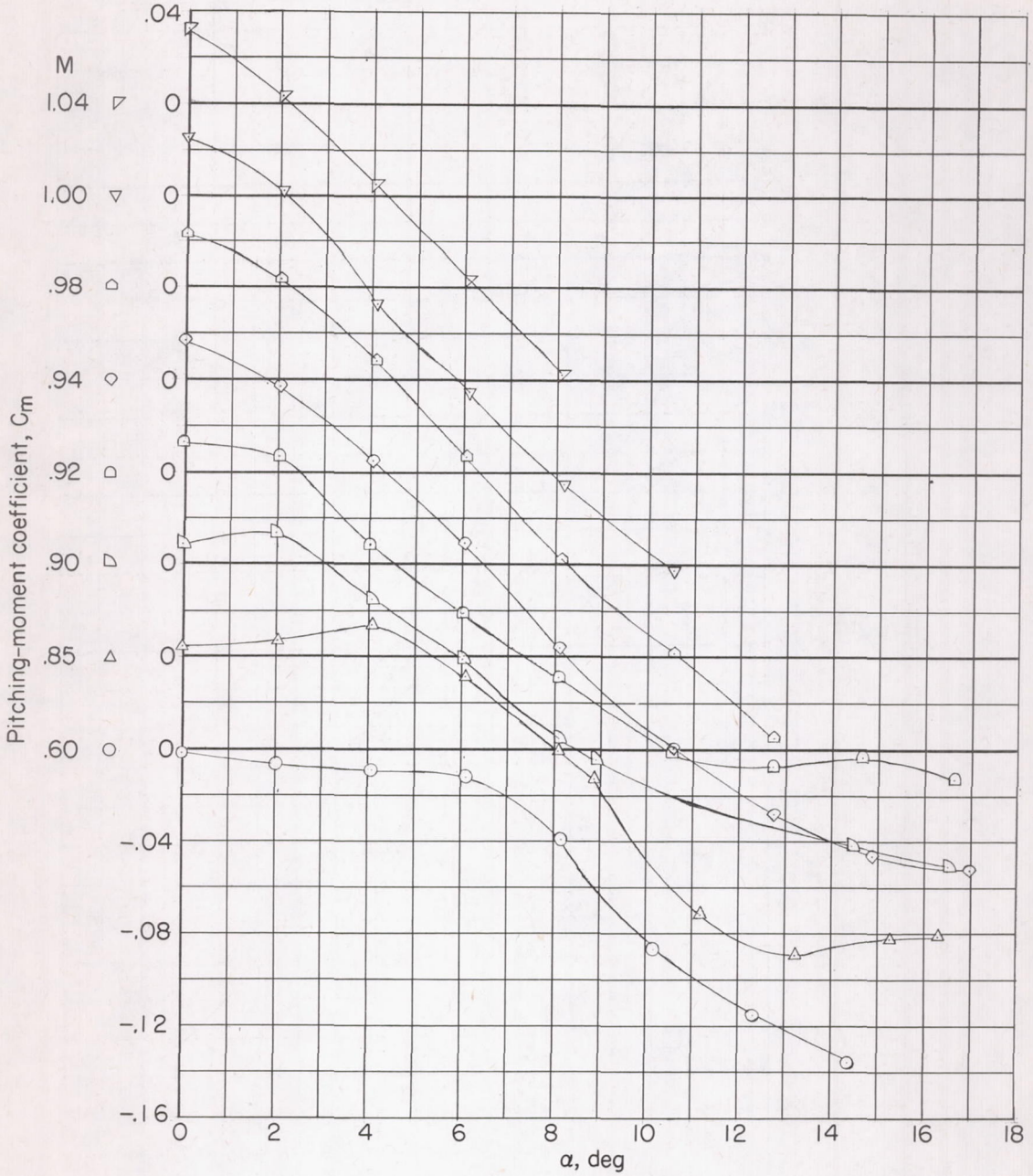

(c) $\frac{h_t}{b/2} = 0.205$; $i_t = 0^\circ$.

Figure 6.- Continued.

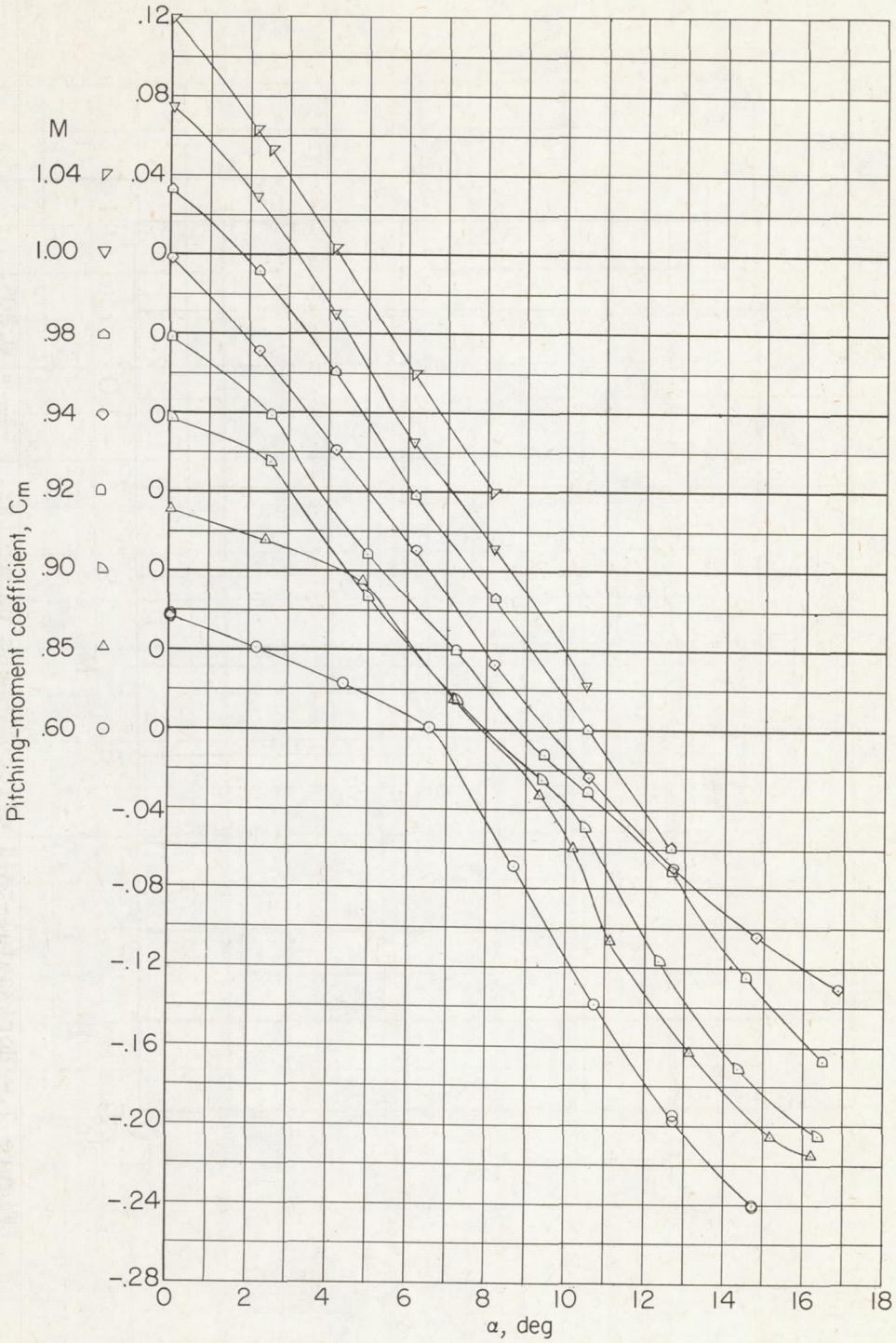

(d) $\frac{h_t}{b/2} = 0.614$; $i_t = -2^{\circ}$.

Figure 6.- Concluded.

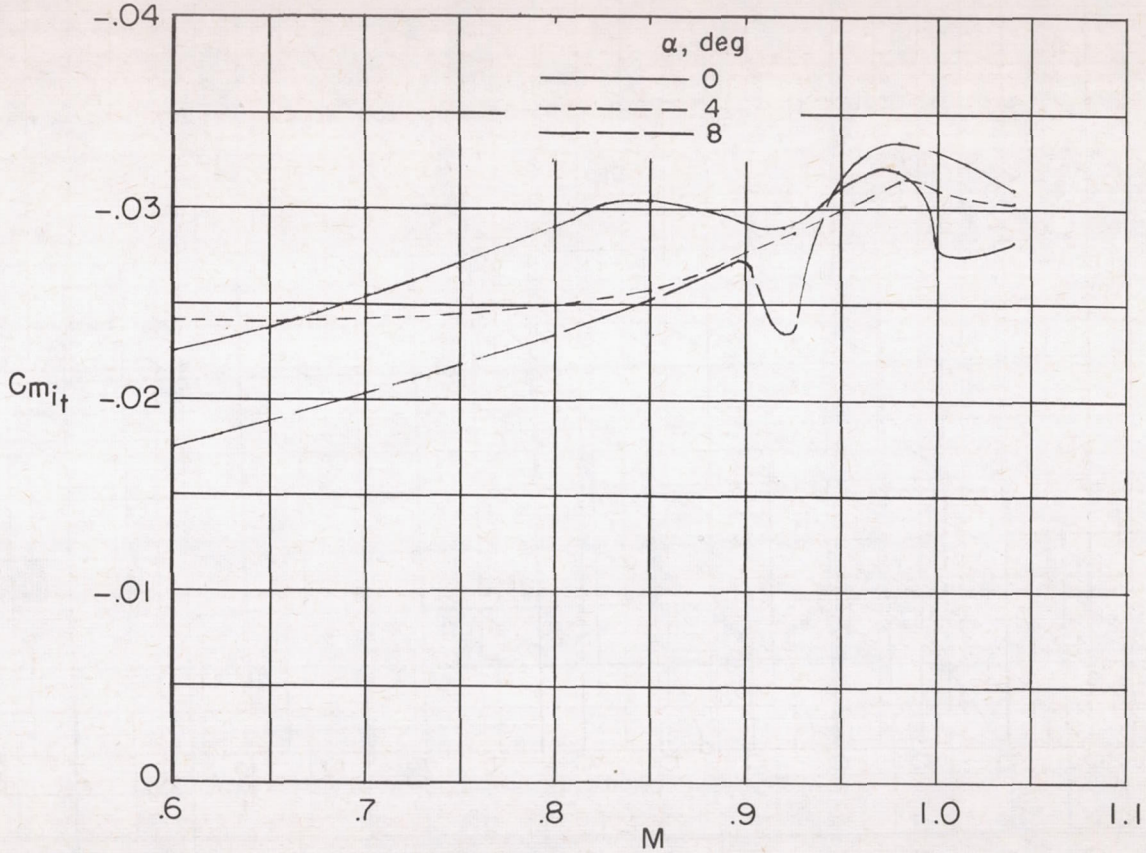

Figure 7.- Horizontal-tail effectiveness parameter. $\frac{h_t}{b/2} = 0.205$.

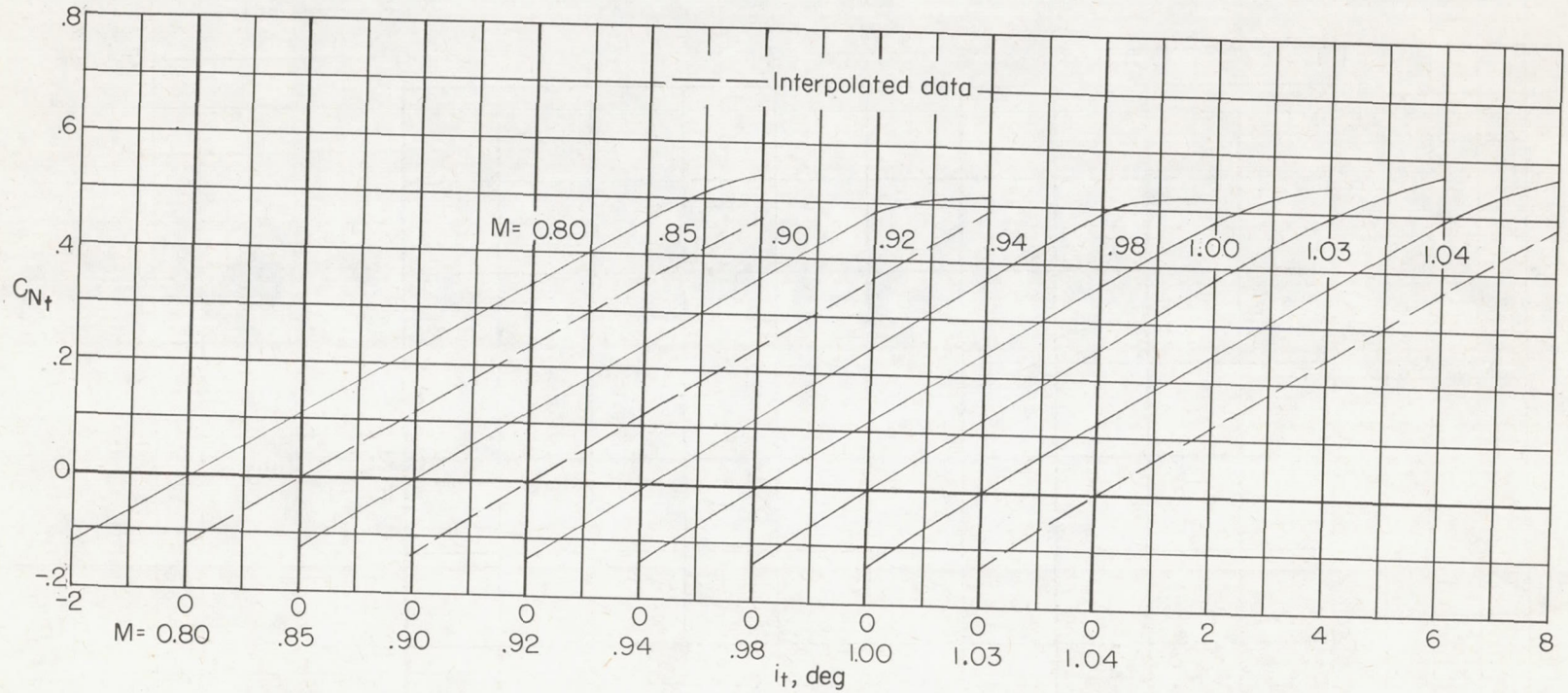

Figure 8.- Variation of horizontal-tail normal-force coefficient with tail incidence.

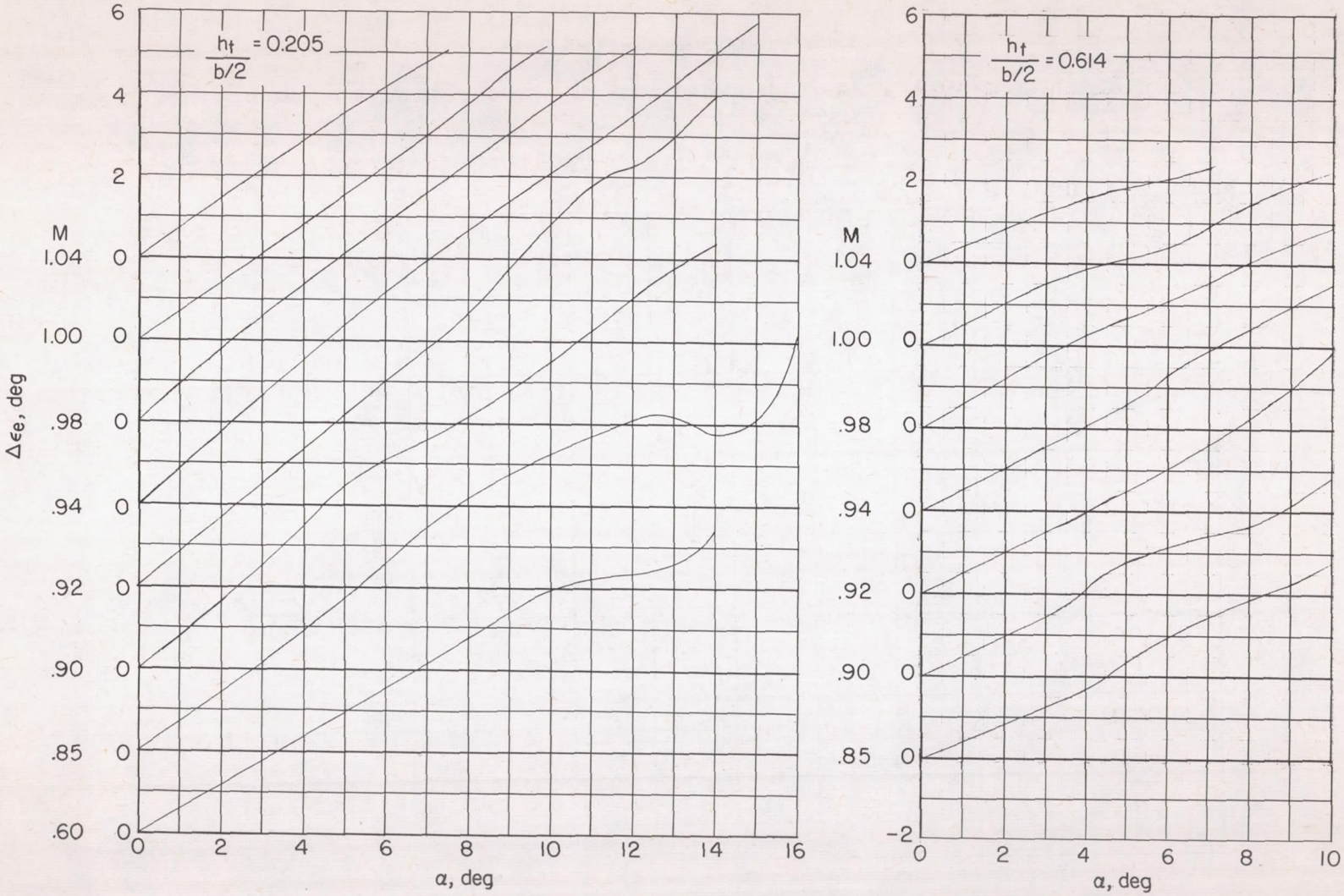

Figure 9.- Variation of effective downwash angle with angle of attack.

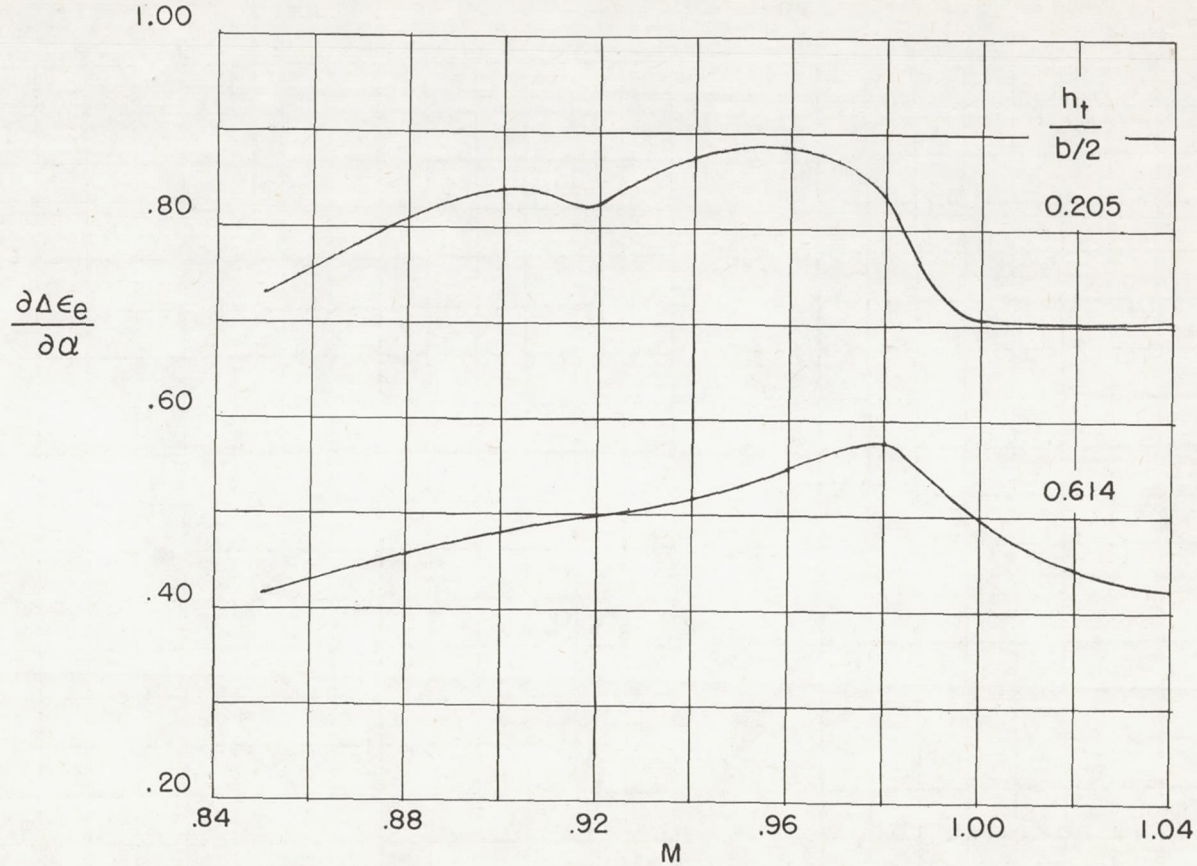

Figure 10.- Variation of downwash parameter $\frac{\partial \Delta \epsilon_e}{\partial \alpha}$ with Mach number for two tail-height locations.

NACA - Langley Field, Va.